Progress In Electromagnetics Research M, Vol. 108, 39–51, 2022

Low-Pass Negative Group Delay Modelling and Experimentation with Tri-Port Resistorless Passive Cross-Circuit

Eric J. R. Sambatra[1], Antonio Jaomiary[2, *], Samuel Ngoho[3], Samar S. Yazdani[4], Nour M. Murad[5], George Chan[6], and Blaise Ravelo[7]

Abstract—This paper introduces an original study of low-pass (LP) negative group delay (NGD) circuit. The family of the proposed passive network cross-topology was rarely investigated in the literature. It acts as a tri-port passive circuit presenting a cross-shaped topology. The present study of tri-port passive circuit is originally based on S-matrix modelling. The identification method of LP-NGD function type is established. The considered passive tri-port topology is innovatively constituted by a resistorless LC-passive network. Thanks to the impedance 3-D matrix modelling, the cross-circuit S-parameters are analytically expressed. Then, the NGD analysis at very low-frequencies is presented. The LP-NGD behavior existence condition of the cross-circuit in function of the L and C components is established. The relevance of the tri-port NGD circuit theory is verified by a proof-of-concept of resistorless cross-circuit. Analytical modelling, simulation, and experimentation confirmed the LP-NGD design feasibility with NGD value of about -2 ns and 6.67 MHz cut-off frequency.

1. INTRODUCTION

The first experimentations of the unfamiliar negative group delay (NGD) effect to non-specialist electronic engineer were realized in 1980s [1, 2]. The NGD existence demonstration in optical wavelength was developed by means of negative group velocity (NGV) dispersive media [3, 4]. Artificial metamaterial structures with possibility to operate with negative refractive group index which implies also the NGD effect were designed.

Despite the remarkable experimental work on the NGD effect, the physical meaning was a fascinating curious question for many researchers. The same effect was verified in early 2000s, with negative refractive index artificial transmission line (TL) metamaterials [5, 6]. However, the metamaterial based NGD circuits are incredibly lossy which can present attenuation more than 30 dB to reach significant NGD values [5, 6]. Because of Kramers-Kronig relation [7], most of NGD passive structure designs need to be accompanied by a transmission loss to have minimum NGD at the expected frequencies. The trade-off between NGD and transmission loss is generally quantified in [8–10]. Nowadays, one of the NGD researcher challenges is to elaborate electronic circuit with lower loss at expected NGD values. To study such RF and microwave circuits, relevant design method developed with S-parameter equivalent modelling is necessary [11].

Then, the NGD microstrip circuit design becomes a research topic attracting RF and microwave and electronic researchers [5–8, 11–20]. Distributed NGD circuit with second order resistive-capacitive

Received 2 November 2021, Accepted 6 January 2022, Scheduled 8 February 2022

* Corresponding author: Antonio Jaomiary (jaomiaryantonio@yahoo.fr).

[1] Institut Supérieur de Technologie (ISTD), BP 509, Antsiranana 201, Madagascar. [2] Ecole Normale Supérieure pour l'Enseignement Technique (ENSET), University of Antsiranana, BP 0, Antsiranana 201, Madagascar. [3] Association Française de Science des Systèmes (AFSCET), Paris 75013, France. [4] Bahria University Karachi Campus, Software Engineering Department, Karachi, Pakistan. [5] PIMENT, Network and Telecom Lab, Institut Universitaire de Technologie, University of La Reunion, Saint Pierre 97410, France. [6] ASM Pacific Technology Ltd., Hong-Kong, China. [7] Nanjing University of Information Science & Technology (NUIST), Nanjing, Jiangsu 210044, China.

topology was proposed [12]. Microwave NGD topologies based on transversal filter approach was introduced [13, 14]. The NGD effects were investigated theoretically and experimentally with various topologies as absorptive bandstop filter [15] and interference technique microstrip circuits [16]. In 2010s, the main challenge was opened on the design of low-attenuation [17] and compact NGD passive circuits [18, 19]. Those low attenuation NGD circuits were expected to be exploited in the microwave areas as the design of a tunable center frequency device [20]. LF NGD topologies constituted by R, L, and C lumped components were also introduced [21, 22]. Based on low-frequency (LF) topologies, it was demonstrated that NGD circuit outputs can propagate in time-advance with the corresponding inputs [21–23]. By taking these different emerging NGD topologies into account, most of electronic engineers were wondering about a simple manner of NGD analysis. Simple classification of elementary NGD circuits was initiated by the analogy between the filter and NGD functions [24–27]. The classes of low-pass (LP) [24, 25], high-pass (HP) [24–26], and stopband [24–27] NGD circuits were proposed.

However, different from the classical electronic functions (filters, amplifiers, antennas, phase shifters, power combiners/dividers), the NGD circuits [3–25] available in the literature are only designed with two-port topologies. By curiosity, we would like to study the design feasibility of tri-port NGD topologies with electrical interconnect circuits [28, 29]. Some rare research works on multi-port LP-NGD topologies [30–33] were recently investigated. Typical three- [30, 31] and four-port [31–33] topologies of bandpass (BP) NGD circuit were proposed. However, the LP-NGD circuit study with resistorless topology remains a challenging and original task. The present paper develops a resistorless cross topology of LP-NGD circuit. The proposed topology is constituted by LC-network. The paper is organized in three main sections as follows:

- Section 2 is focused on the tri-port cross topology under investigation. The S-matrix modelling will be expressed from impedance or Z-matrix.
- Section 3 elaborates the LP-NGD theorization of the original resistorless topology.
- Section 4 discusses the simulation and experimental validation with a proof-of-concept (PoC).
- Then, Section 5 is the final conclusion of the paper.

2. TOPOLOGICAL DESCRIPTION AND *S*-MATRIX MODELLING

The present section describes the three-port cross-topology. The S-matrix model by means of Z-matrix will be established.

2.1. Description of the Tri-Port Cross-Topology

The LP-NGD cross-topology is only composed of inductor and capacitor elements. Fig. 1 introduces the general topology of the tri-port passive cell constituted by three series impedances represented by $Z_{k=\{1,2,3\}}$ and Z-shunt admittance through node M. It acts as a 3-ports circuit fed by nodes $M_{k=\{1,2,3\}}$.

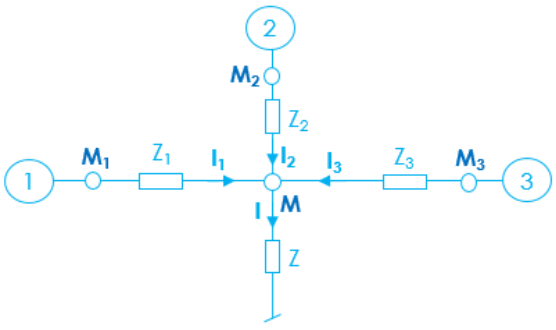

Figure 1. Cross-topology under study.

Each series branch is traversed by currents I_k and the shunt branch by:

$$I_1(s) + I_2(s) + I_3(s) = 0 \tag{1}$$

where $s = j\omega$ is the Laplace variable and the angular frequency, ω. The cross-topology will be analytically modelled in the following subsection.

2.2. *S*-Matrix Modelling

The cross-topology can be fundamentally modelled from the generalized Ohm's law:

$$\begin{bmatrix} V_1(s) \\ V_2(s) \\ V_3(s) \end{bmatrix} = [Z(s)] \times \begin{bmatrix} I_1(s) \\ I_2(s) \\ I_3(s) \end{bmatrix}. \tag{2}$$

Based on circuit and system theory, the associated Z-matrix is represented by:

$$[Z(s)] = \begin{bmatrix} Z_1(s) + Z(s) & Z(s) & Z(s) \\ Z(s) & Z_2(s) + Z(s) & Z(s) \\ Z(s) & Z(s) & Z_3(s) + Z(s) \end{bmatrix}. \tag{3}$$

By denoting $R_0 = 50\,\Omega$, the reference impedance, the corresponding S-parameters are given by:

$$[S(s)] = \{[Z(s)] - R_0\,[Id_3]\} \times \{[Z(s)] + R_0\,[Id_3]\}^{-1}. \tag{4}$$

where the 3-D identity matrix:

$$[Id_3] = \begin{bmatrix} 1 & 0 & 0 \\ 0 & 1 & 0 \\ 0 & 0 & 1 \end{bmatrix}. \tag{5}$$

Thanks to the relationship in Eq. (4), the S-parameter coefficients were calculated in function of the cross-circuit parameters. The following paragraph explores the analytical results.

2.3. Reflection and Transmission Coefficient Expressions of the Resistorless Cross-Circuit

The resistorless circuit is considered as an LC-network with inductor and capacitor elements defined by, respectively:

$$Z_{m=\{1,2,3\}}(s) = L_m\, s \tag{6}$$

$$Z(s) = \frac{1}{Cs}. \tag{7}$$

The reflection coefficients are:

$$S_{mm}(s) = \frac{CL_1L_2L_3s^4 - \sum_{k=1}^{3} n_k^{mm} s^k - R_0^2}{\sum_{k=0}^{4} d_k s^k} \tag{8}$$

with:

$$\begin{cases} n_1^{11} = R_0(2L_1 - R_0^2C) \\ n_2^{11} = R_0^2C(L_2 + L_3 - L_1) + L_1L_2 + L_3(L_1 + L_2) \\ n_3^{11} = R_0C\,[L_1L_2 + (L_1 - L_2)L_3)] \end{cases} \tag{9}$$

$$\begin{cases} n_1^{22} = R_0(2L_2 - R_0^2C) \\ n_2^{22} = R_0^2C(L_1 - L_2 + L_3) + L_1L_2 + L_3(L_1 + L_2) \\ n_3^{22} = R_0C\,[L_1L_3 - L_2(L_1 + L_3)] \end{cases} \tag{10}$$

$$\begin{cases} n_1^{33} = R_0(2L_3 - R_0^2C) \\ n_2^{33} = R_0^2C(L_1 + L_2 - L_3) - L_1L_2 - (L_1 + L_2)L_3 \\ n_3^{33} = R_0C\,[(L_1 + L_2)L_3 - L_1L_2] \end{cases} \tag{11}$$

$$\begin{cases} d_0 = 3R_0^2 \\ d_1 = R_0\left[R_0^2C + 2(L_1 + L_2 + L_3)\right] \\ d_2 = L_1L_2 + L_3(L_1 + L_2) + R_0^2C(L_1 + L_2 + L_3) \\ d_3 = R_0C\left[L_1L_2 + L_3(L_1 + L_2)\right] \\ d_4 = CL_1L_2L_3 \end{cases} \tag{12}$$

By taking m, $n = \{1, 2, 3\}$ with $m \neq n$, the transmission coefficients can be written as:

$$S_{mn}(s) = \frac{2R_0(n_{mn}^s + R_0)}{\sum_{k=0}^{4} d_k s^k} \tag{13}$$

with:

$$\begin{cases} n_{21} = L_3 \\ n_{31} = L_2 \\ n_{32} = L_1 \end{cases} \tag{14}$$

Knowing the S-matrix model, the LP-NGD analysis will be developed in the next section.

3. TRI-PORT CIRCUIT LP-NGD THEORY APPLIED TO CROSS-TOPOLOGY

This section describes the cross-topology LP-NGD theory. After the S-matrix modelling, the LP-NGD analysis will be developed.

3.1. LP-NGD Function Ideal Specifications

The LP-NGD function analysis is based on the frequency dependent magnitude:

$$S_{mn}(\omega) = |S_{mn}(j\omega)| \tag{15}$$

and phase:

$$\varphi_{mn}(\omega) = \arg\left[S_{mn}(j\omega)\right]. \tag{16}$$

The associated GD response is defined by:

$$GD_{mn}(\omega) = \frac{-\partial\varphi_{mn}(\omega)}{\partial\omega}. \tag{17}$$

From this GD definition, the corresponding electronic circuit can be assumed as a typical NGD function if there is an angular frequency, $\omega_x > 0$, where:

$$GD(\omega_x) < 0. \tag{18}$$

The NGD cut-off frequencies are the roots of equation:

$$GD(\omega) = 0. \tag{19}$$

Fig. 2 represents the LP-NGD function ideal responses:

$$GD(\omega \approx 0) = GD_n < 0 \tag{20}$$

and NGD cut-off angular frequency, ω_0. According to the expected attenuation loss and matching limitations, $S_{21\,\min}$ and $S_{11\,\max}$, in the NGD bandwidth ($\omega \leq \omega_n$), we can suppose that the S-parameter magnitudes respect the conditions:

$$S_{mn} > \min(S_{mn}) \tag{21}$$

$$S_{mm} > \max(S_{mm}) \tag{22}$$

3.2. LF NGD Analyses

At LF ($\omega \approx 0$), the reflection and transmission coefficients established in Equations (8) and (13) will become:

$$\begin{cases} S_{mm}(\omega \approx 0) = |S_{mm}(s \approx 0)| = R_0^2/d_0 = 1/3 \\ S_{mn}(\omega \approx 0) = |S_{mn}(s \approx 0)| = 2R_0^2/d_0 = 2/3 \end{cases}. \tag{23}$$

It is noteworthy that the S-matrix does not depend on the cross-topology inductive and capacitive parameters. The key step of this analytical investigation is based on the intermediate calculation of the phase and GD from expressions (16) and (17), respectively. After intensive mathematical calculations, we can theoretically demonstrate that GD_{mn} at LF between the transmission ports m and n of the cross-topology introduced in Fig. 1 are given by the following expressions:

$$GD_{21}(\omega \approx 0) = R_0C + \frac{2(L_1 + L_2) - L_3}{3R_0} \tag{24}$$

$$GD_{31}(\omega \approx 0) = R_0C + \frac{2(L_1 + L_3) - L_2}{3R_0} \tag{25}$$

$$GD_{32}(\omega \approx 0) = R_0C + \frac{2(L_3 + L_2) - L_1}{3R_0}. \tag{26}$$

By denoting $p \neq \{m,n\}$, this GD can be compactly rewritten as:

$$GD_{mn}(\omega \approx 0) = R_0^2C + \frac{2(L_m + L_n) - L_p}{3R_0}. \tag{27}$$

From this last equation, we remark that the capacitive shunt element is responsible for the positive GD contribution. In the case of transmission from different port$_m$ to port$_n$, the NGD effect is mainly induced by the opposite inductive element L_p.

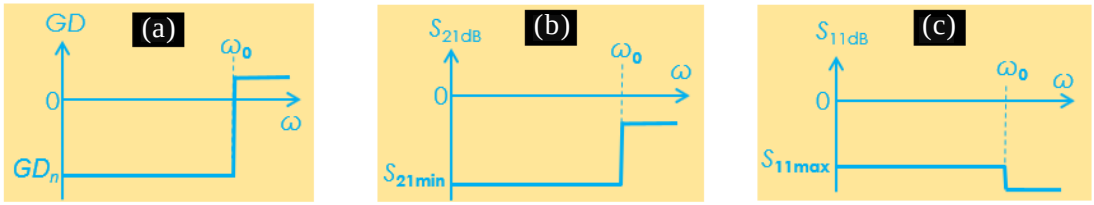

Figure 2. LP-NGD function (a) GD, (b) transmission coefficient and (c) reflection coefficient ideal responses.

3.3. LP-NGD Existence Condition and Synthesis Equation of Inductive Elements

The quantity "-L_p" in Equation (27) enables one to think that the resistorless cross-topology can behave as LP-NGD function. The mathematical existence condition is:

$$\begin{cases} GD_{mn}(\omega \approx 0) < 0 \\ S_{mn}(\omega \approx 0) \neq 0 \end{cases}. \tag{28}$$

It means that the cross-topology GD between port m and port n can be negative under the condition:

$$L_p \geq R_0^2C + 2(L_m + L_n). \tag{29}$$

Supposing given the capacitor, the inductors can be calculated in function of desired NGD value ($GD_0 < 0$), by the equation:

$$2(L_m + L_n) - L_p = R_0(3GD_0 - R_0C). \tag{30}$$

This relation can also be rewritten as:

- For NGD corresponding to transmission between port$_1$ and port$_2$:

$$L_3 = 2(L_1 + L_2) - R_0(3GD_0 - R_0C). \tag{31}$$

- For NGD corresponding to transmission between port$_1$ and port$_3$:

$$L_2 = 2(L_1 + L_3) - R_0(3GD_0 - R_0C). \tag{32}$$

- For NGD corresponding to transmission between port$_2$ and port$_3$:

$$L_1 = 2(L_2 + L_3) - R_0(3GD_0 - R_0C). \tag{33}$$

3.4. LP-NGD Cut-Off Frequencies

Under the particular condition:

$$L_p \gg \sup(L_n, L_m) \tag{34}$$

the transmission coefficient given in Equation (13) becomes:

$$S_{mn}(s) \approx \frac{2(L_p^s + R_0)}{R_0(L_pCs^2 + 3) + R_0^2Cs}. \tag{35}$$

The equivalent detailed quantities corresponding to transmission between port$_2$ and port$_1$, port$_3$ and port$_1$, and port$_3$ and port$_2$ can be expressed as, respectively:

$$S_{21}(s) \approx \frac{2(L_3^s + R_0)}{R_0(L_3Cs^2 + 3) + R_0^2Cs} \tag{36}$$

$$S_{31}(s) \approx \frac{2(L_2^s + R_0)}{R_0(L_2Cs^2 + 3) + R_0^2Cs} \tag{37}$$

$$S_{32}(s) \approx \frac{2(L_1^s + R_0)}{R_0(L_1Cs^2 + 3) + R_0^2Cs}. \tag{38}$$

In this case, the cross-circuit NGD cut-off angular frequency can be estimated by:

$$\omega_0^{mn} \approx \frac{\sqrt{\sqrt{(2L_p + R_0^2C)(2L_p + 25R_0^2C)} - 2L_p - 7R_0^2C}}{2L_p\sqrt{C}}. \tag{39}$$

Accordingly, the NGD cut-off frequencies corresponding to transmission between port$_2$ and port$_1$, port$_3$ and port$_1$, and port$_3$ and port$_2$ can be expressed as, respectively:

$$\omega_0^{21} \approx \frac{\sqrt{\sqrt{(2L_3 + R_0^2C)(2L_3 + 25R_0^2C)} - 2L_3 - 7R_0^2C}}{2L_3\sqrt{C}} \tag{40}$$

$$\omega_0^{31} \approx \frac{\sqrt{\sqrt{(2L_2 + R_0^2C)(2L_2 + 25R_0^2C)} - 2L_2 - 7R_0^2C}}{2L_2\sqrt{C}} \tag{41}$$

$$\omega_0^{32} \approx \frac{\sqrt{\sqrt{(2L_1 + R_0^2C)(2L_1 + 25R_0^2C)} - 2L_1 - 7R_0^2C}}{2L_1\sqrt{C}}. \tag{42}$$

To verify the LP-NGD theory feasibility, a tri-port cross-circuit prototype will be considered in the next section.

4. SIMULATED AND EXPERIMENTAL VALIDATIONS

The present section deals with the tri-port cross-topology LP-NGD validation. The synthesis, design, and implementation of the PoC are described. After experimental setup introduction, the modeled, simulated, and measured results will be examined.

4.1. Description of Cross-Circuit PoC

Similar to classical electronic circuits, the tri-port cross-circuit prototype was designed with inductor and capacitor lumped components. It was implemented on FR4 dielectric substrate. Fig. 3(a) shows the cross-circuit schematic designed with ADS® simulator from Keysight Technologies®. The fabricated circuit shown in Fig. 3(b) has a physical size of 30 mm × 50 mm.

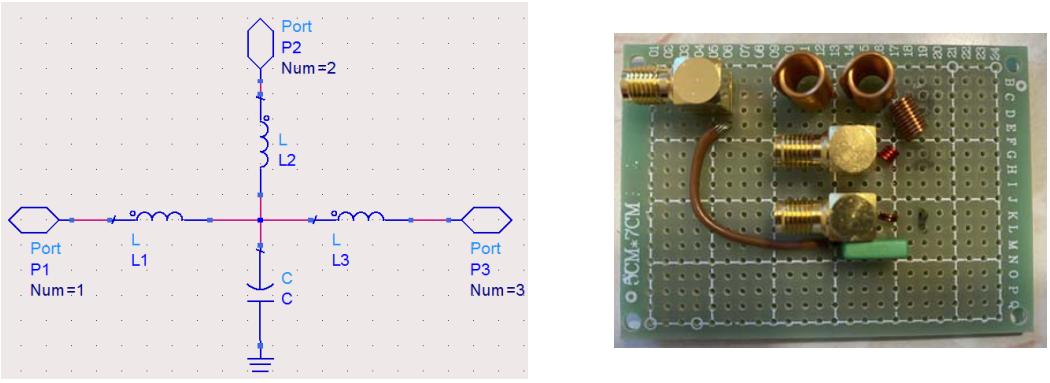

(a) (b)

Figure 3. (a) Schematic and (b) photo of the fabricated NGD cross-circuit.

The substrate physical characteristics are addressed in the first row of Table 1. The circuit design was performed with the application of synthesis Equation (30) for the desired LF NGD, $GD_{21}(f \approx 0) = GD_0 = -2\,\text{ns}$. The electrical component parameters are indicated in the second row of Table 1. Similar to the RF classical circuits, the cross-circuit test is based on the three-port S-parameter measurement.

Table 1. Parameters of the cross-circuit prototype.

Structure	Description	Parameters	Values
Substrate	Relative permittivity	ε_r	4.5
	Loss tangent	$\tan(\delta)$	0.02
	Thickness	h	1.6 mm
Lumped components	Inductor	L_1	10 nH
		L_2	15 nH
		L_3	620 nH
	Capacitor	C	100 pF

4.2. Experimental Setup of the Tri-Port Circuit Prototype

Our tri-port cross-circuit prototype is a typical RF passive device. The proposed LP-NGD characterization is fundamentally performed based on the S-parameter modelling. Similar to classical RF circuits, the experimental investigation was carried out by considering a three-port testing technique. Fig. 4 highlights the experimental setup.

The measurement was performed with a Vector Network Analyzer (VNA) referenced ENA Series E5071C from Keysight Technologies® which has frequency band delimited from 9 kHz to 8.5 GHz. The S-parameter measurement test was made under SOLT calibration. The obtained validation results will be discussed in the following section.

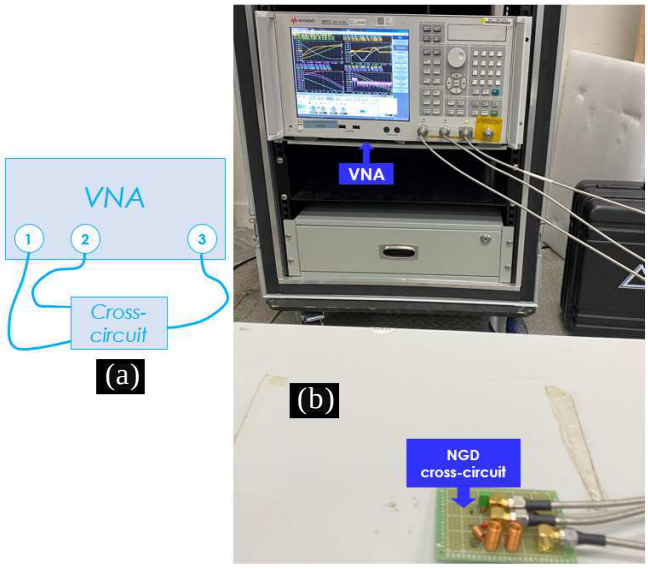

Figure 4. (a) Illustrative diagram and (b) photograph of the experimental setup with the NGD cross-circuit.

4.3. Validation Results of LP-NGD Aspect with a Resistorless Cross Circuit Prototype

The cross-circuit experimental validation consists in the comparison between the calculated, simulated (ADS®), and measured results from 10 kHz to 60 MHz. The calculated results were obtained with MATLAB® by programming the transmission and reflection coefficients established in Equations (8) and (13), respectively. The S-parameter magnitudes of the cross-circuit PoC are displayed in Fig. 5. The measured S-parameter slight divergence is mainly due to the component inaccuracies and parasitic effects. The reflection and transmission coefficients between port_1 and port_2 are in very good agreement. S_{21} reach their maximal values between 25 MHz and 35 MHz, and S_{11} present their minimal values between 15 MHz and 25 MHz.

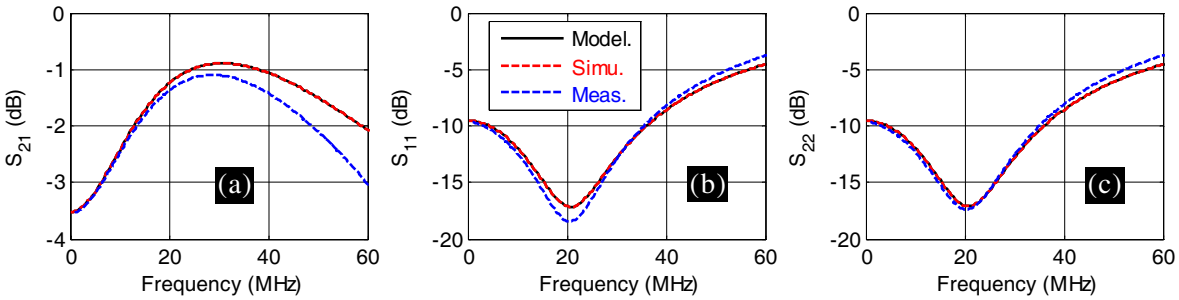

Figure 5. Calculated, simulated, and measured (a) S_{21}, (b) S_{11} and (b) S_{22} of the cross-circuit prototype shown in Fig. 4.

To verify the LP-NGD behavior, the three GD responses between the cross-circuit access ports are also plotted in Fig. 6. The measured GD observed discrepancies are mainly due to tolerances and parasitic effects of the employed components, and the measurement systematic errors. It can be understood from Fig. 6(a) that the tested cross-circuit presents an LP-NGD response between port_1-port_2. However, the GDs between port_1-port_3 and port_2-port_3 which are shown by Fig. 6(b) and Fig. 6(c), respectively, are always positive.

Table 2 presents the comparison of the LP-NGD specifications from the calculation, simulation, and

Table 2. Comparison of calculated, simulated and measured cross-circuit LP-NGD specifications.

Approach	f_0	$GD_{21}(f \approx 0)$	FoM	$S_{21}(f \approx 0)$	$S_{11}(f \approx 0)$
Calc.	6.67 MHz	−1.998 ns	13.327×10^{-3}	−3.521 dB	−9.541 dB
Simu.	6.67 MHz	−1.994 ns	13.3×10^{-3}	−3.522 dB	−9.542 dB
Meas.	8 MHz	−1.78 ns	14.26×10^{-3}	−3.534 dB	−9.668 dB

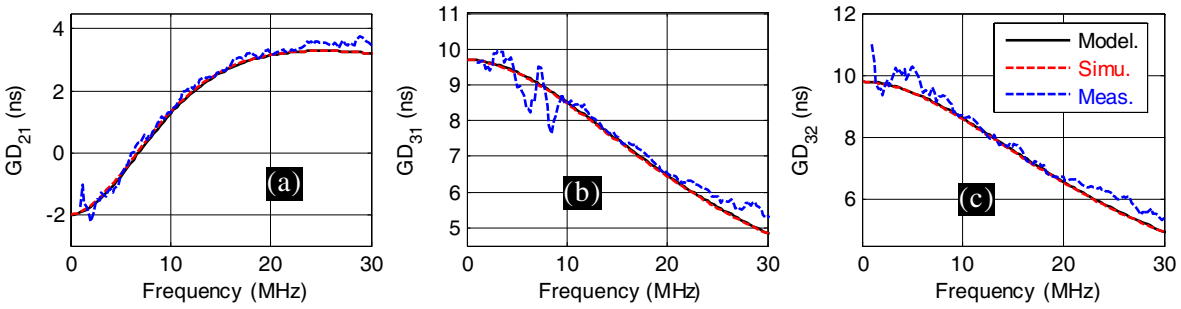

Figure 6. Calculated, simulated, and measured (a) GD_{21}, (b) GD_{31} and (c) GD_{32} of the cross-circuit prototype shown in Fig. 4.

measurement results. The LP-NGD $FoM = f_0 \cdot |GD_{21}(f \approx 0)|$ which represents the NGD value-NGD bandwidth product is also indicated in Table 2. In the perspective of this work, the FoM achieved with a resistorless network can be compared to the achievable FoM of a simple single-stage resistor-based circuit, for the same amplitude variation at cut-off (around 1 dB) and the maximum out-of-band gain (2.5 dB roughly).

4.4. Sensitivity Analyses (SAs)

The cross-circuit SAs were performed by considering inductor and capacitor relative variations of +/−10%. The SAs focus on the cross-circuit parameters corresponding to the transmission between port$_1$-port$_2$, GD_{21}, S_{11}, and S_{21}. Fig. 7(a), Fig. 7(b), and Fig. 7(c) display the surface plots of the computed GD, reflection, and transmission coefficient results. The computed results are represented with respect to the frequency and variation of inductor element L_1 which varies linearly from $L_{1\,\min} = 9$ nH to $L_{1\,\max} = 11$ nH. Fig. 8(a), Fig. 8(b), and Fig. 8(c) represent the similar results for the case of inductor element L_2, varied from $L_{2\,\min} = 13.5$ nH to $L_{2\,\max}$=16.5 nH. Fig. 9(a), Fig. 9(b), and Fig. 9(c) show the surface plots of the GD, reflection, and transmission coefficients in the case of L_3 varied linearly from $L_{3\,\min} = 540$ nH to $L_{3\,\max} = 640$ nH. Fig. 10(a), Fig. 10(b), and Fig. 10(c) highlight the variation of GD, reflection, and transmission coefficients with also surface plot. In this last case, the SA is applied to the variation of the capacitor element C, from $C_{\min} = 90$ pF to $C_{\max} = 110$ pF. We can

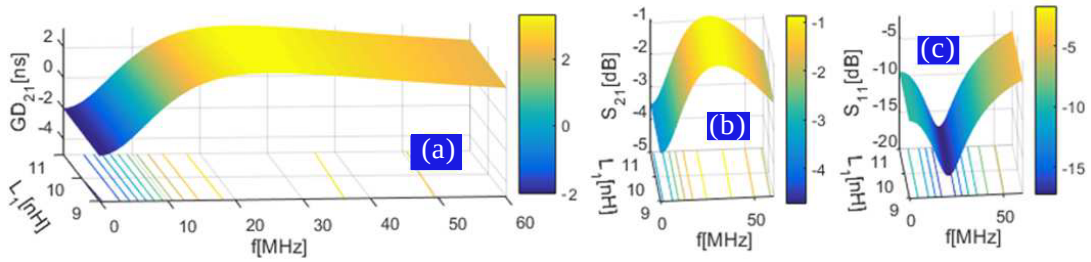

Figure 7. Surface plots of (a) GD_{21}, (b) S_{21} and (c) S_{11} versus (f, L_1).

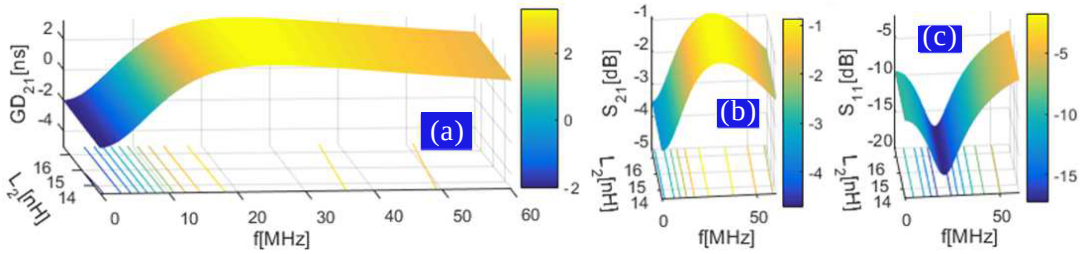

Figure 8. Surface plots of (a) GD_{21}, (b) S_{21} and (c) S_{11} versus (f, L_2).

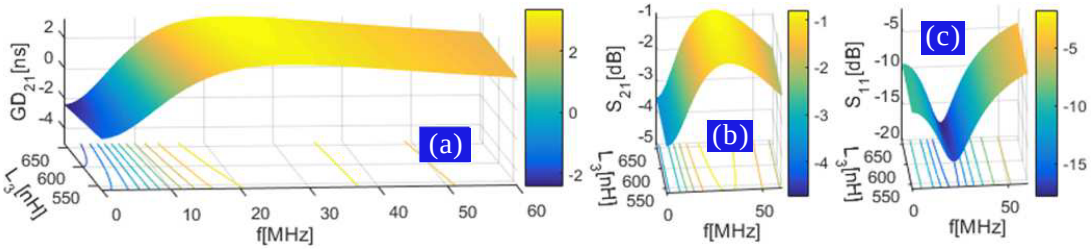

Figure 9. Surface plots of (a) GD_{21}, (b) S_{21} and (c) S_{11} versus (f, L_3).

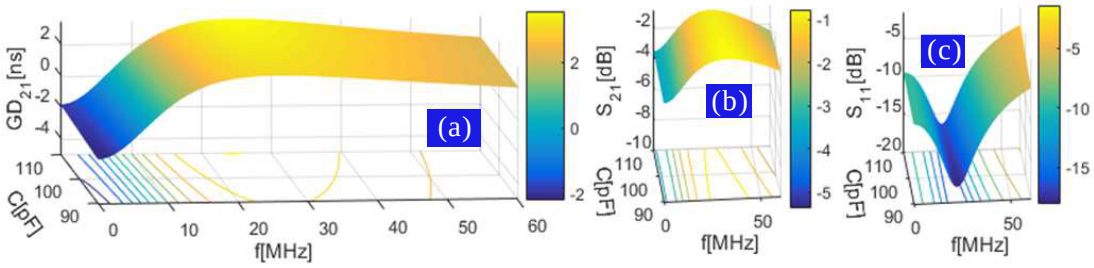

Figure 10. Surface plots of (a) GD_{21}, (b) S_{21} and (c) S_{11} versus (f, C).

underline that the LP-NGD behavior is still verified despite the relative variation because condition (14) remains satisfied. The minimal and maximal values of the NGD cut-off frequency and the GD value at LF for each result of SAs are indicated in Table 3. Moreover, S_{21} and S_{11} conserve their behaviors in the NGD frequency band for the four cases of SAs. As the tested cross-circuit constituting components satisfy condition $L_3 \gg \sup\{L_1, L_2\}$, the variation influences of L_1 and L_2 can be neglected on the LP-NGD behavior. However, with the 10% tolerance of the capacitor, the NGD cut-off frequency and GD at LF present respectively 15.3% and 8.3% relative variations.

Table 3. Minimal and maximal values of NGD cut-off frequencies and GD values.

Considered SA parameter	$f_{0\,\min}$	$f_{0\,\max}$	$GD_{21\,\min}(f \approx 0)$	$GD_{21\,\max}(f \approx 0)$
L_1	6.67 MHz	7 MHz	−2.01 ns	−1.98 ns
L_2	6.67 MHz	6.67 MHz	−2.02 ns	−1.98 ns
L_3	6.67 MHz	6.67 MHz	−2.4 ns	−1.6 ns
C	6.51 MHz	7.59 MHz	−2.16 ns	−1.83 ns

5. CONCLUSION

An original study of three-port circuit operating as LP-NGD function type is investigated. The developed study elaborates the NGD behavior of topology represented by a cross-shape circuit. Different from the recent NGD investigation on tri-port topology, the present one is essentially constituted by a resistorless LC-network.

An innovative analytical approach on LP-NGD function identification is developed. The 3-D S-matrix model of the cross-topology is established. The LP-NGD analysis and existence condition are theoretically described in function of the lumped LC component parameters. A PoC of lumped cross-circuit prototype was designed, simulated, fabricated, and tested to validate the LP-NGD function. Calculation, simulation, and measurement results in very good correlation confirm the LP-NGD behavior of the signal transmitted between port_1 and port_2 of the cross-circuit prototype. The influences of each component $+/-10\%$ tolerance on the NGD response are studied by the SAs.

The present resistorless cross-topology has a significant benefit compared to [8, 10] in terms of 3-dB bandwidth designs with higher out-of-band gains (over 20 dB) which may induce important amplitude/phase distortion metric. This distortion stays quite low in the present research work which has roughly 1-dB bandwidth and only 2.5 dB out-of-band gain.

By using an adequate equalization technique [34, 35], the three-port NGD circuit can be used for reducing the GD effects [36, 37] in an electronic and communication system.

REFERENCES

1. Chu, S. and S. Wong, "Linear pulse propagation in an absorbing medium," *Phys. Rev. Lett.*, Vol. 48, 738–741, 1982.
2. Ségard, B. and B. Macke, "Observation of negative velocity pulse propagation," *Phys. Lett. A*, Vol. 109, 213–216, 1985.
3. Macke, B. and B. Ségard, "Propagation of light-pulses at a negative group-velocity," *Eur. Phys. J. D*, Vol. 23, 125–141, 2003.
4. Munday, J. N. and W. M. Robertson, "Observation of negative group delays within a coaxial photonic crystal using an impulse response method," *Optics Communications*, Vol. 273, No. 1, 32–36, 2007.
5. Eleftheriades, G. V., O. Siddiqui, and A. K. Iyer, "Transmission line for negative refractive index media and associated implementations without excess resonators," *IEEE Microw. Wireless Compon. Lett.*, Vol. 13, No. 2, 51–53, Feb. 2003.
6. Siddiqui, O. F., M. Mojahedi, and G. V. Eleftheriades, "Periodically loaded transmission line with effective negative refractive index and negative group velocity," *IEEE Trans. Antennas Propagat.*, Vol. 51, No. 10, 2619–2625, Oct. 2003.
7. Bolda, L., R. Y. Chiao, and J. C. Garrison, "Two theorems for the group velocity in dispersive media," *Phys. Rev. A, Gen. Phys.*, Vol. 48, No. 5, 3890–3894, Nov. 1993.
8. Macke, B., B. Ségard, and F. Wielonsky, "Optimal superluminal systems," *Phys. Rev. E*, Vol. 72, 035601(R), 1–4, Sep. 2005.
9. Kandic, M. and G. Bridges, "Asymptotic limits of negative group delay in active resonator-based distributed circuits," *IEEE Trans. Circuits Syst. I: Regular Papers*, Vol. 58, No. 8, 1727–1735, Aug. 2011.
10. Kandic, M. and G. Bridges, "Negative group delay prototype filter based on cascaded second order stages implemented with Sallen-Key topology," *Progress In Electromagnetics Research B*, Vol. 94, 1–18, Sep. 2021.
11. Markley, L. and G. V. Eleftheriades, "Quad-band negative-refractive-index transmission-line unit cell with reduced group delay," *Electronics Letters*, Vol. 46, No. 17, 1206–1208, Aug. 2010.
12. Ahn, K.-P., R. Ishikawa, A. Saitou, and K. Honjo, "Synthesis for negative group delay circuits using distributed and second-order RC circuit configurations," *IEICE Trans. on Electronics*, Vol. E92-C, No. 9, 1176–1181, 2009.

13. Wu, C.-T.-M. and T. Itoh, "Maximally flat negative group-delay circuit: A microwave transversal filter approach," *IEEE Trans. Microw. Theory Techn.*, Vol. 62, No. 6, 1330–1342, Jun. 2014.
14. Zhang, T., R. Xu, and C. M. Wu, "Unconditionally stable non-foster element using active transversal-filter-based negative group delay circuit," *IEEE Microw. Wireless Compon. Lett.*, Vol. 27, No. 10, 921–923, Oct. 2017.
15. Qiu, L.-F., L.-S. Wu, W.-Y. Yin, and J.-F. Mao, "Absorptive bandstop filter with prescribed negative group delay and bandwidth," *IEEE Microw. Wireless Compon. Lett.*, Vol. 27, No. 7, 639–641, Jul. 2017.
16. Wang, Z., Y. Cao, T. Shao, S. Fang, and Y. Liu, "A negative group delay microwave circuit based on signal interference techniques," *IEEE Microw. Wireless Compon. Lett.*, Vol. 28, No. 4, 290–292, Apr. 2018.
17. Liu, G. and J. Xu, "Compact transmission-type negative group delay circuit with low attenuation," *Electronics Letters*, Vol. 53, No. 7, 476–478, Mar. 2017.
18. Shao, T., Z. Wang, S. Fang, H. Liu, and S. Fu, "A compact transmission line self-matched negative group delay microwave circuit," *IEEE Access*, Vol. 5, No. 1, 22836–22843, Oct. 2017.
19. Shao, T., S. Fang, Z. Wang, and H. Liu, "A compact dual-band negative group delay microwave circuit," *Radio Engineering*, Vol. 27, No. 4, 1070–1076, Dec. 2018.
20. Chaudhary, G. and Y. Jeong, "Tunable center frequency negative group delay filter using coupling matrix approach," *IEEE Microw. Wireless Compon. Lett.*, Vol. 27, No. 1, 37–39, 2017.
21. Mitchell, M. W. and R. Y. Chiao, "Negative group delay and "fronts" in a causal system: An experiment with very low frequency bandpass amplifiers," *Phys. Lett. A*, Vol. 230, Nos. 3–4, 133–138, Jun. 1997.
22. Mitchell, M. W. and R. Y. Chiao, "Causality and negative group-delays in a simple bandpass amplifier," *Am. J. Phys.*, Vol. 66, 14–19, 1998.
23. Wan, F., J. Wang, B. Ravelo, J. Ge, and B. Li, "Time-domain experimentation of NGD active RC-network cell," *IEEE Trans. Circuits and Systems II: Express Briefs*, Vol. 66, No. 4, 562–566, Apr. 2019.
24. Ravelo, B., "Similitude between the NGD function and filter gain behaviours," *Int. J. Circ. Theor. Appl.*, Vol. 42, No. 10, 1016–1032, Oct. 2014.
25. Ravelo, B., "First-order low-pass negative group delay passive topology," *Electron. Lett.*, Vol. 52, No. 2, 124–126, Jan. 2016.
26. Ravelo, B., "High-pass negative group delay RC-network impedance," *IEEE Trans. CAS II: Express Briefs*, Vol. 64, No. 9, 1052–1056, Sept. 2017.
27. Fenni, S., F. Haddad, K. Gorshkov, B. Tishchuk, A. Jaomiary, F. Marty, G. Chan, M. Guerin, W. Rahajandraibe, and B. Ravelo, "AC low-frequency characterization of stop-band negative group delay circuit," *Progress In Electromagnetics Research C*, Vol. 115, 261–276, 2021.
28. Ravelo, B., O. Maurice, and S. Lalléchère, "Asymmetrical 1 : 2 Y-tree interconnects modelling with Kron-Branin formalism," *Electronics Letters*, Vol. 52, No. 14, 1215–1216, Jul. 2016.
29. Ravelo, B., "Behavioral model of symmetrical multi-level T-tree interconnects," *Progress In Electromagnetics Research B*, Vol. 41, 23–50, 2012.
30. Wan, F., Y. Liu, J. Nebhen, Z. Xu, G. Chan, S. Lalléchère, R. Vauche, W. Rahajandraibe, and B. Ravelo, "Bandpass negative group delay theory of fully capacitive Δ-network," *IEEE Access*, Vol. 9, No. 1, 62430–62445, Apr. 2021.
31. Nebhen, J. and B. Ravelo, "Bandpass NGD analysis of symmetric lumped Y-tree via tensorial analysis of networks formalism," *Journal of Electromagnetic Waves and Applications*, Vol. 35, No. 16, 2125–2140, 2021.
32. Ravelo, B., F. Wan, J. Nebhen, G. Chan, W. Rahajandraibe, and S. Lalléchère, "Bandpass NGD TAN of symmetric H-tree with resistorless lumped-network," *IEEE Access*, Vol. 9, 41383–41396, Mar. 2021.

33. Li, N., F. Wan, and B. Ravelo, "Analytical modelling of H-shape distributed topology with bandpass negative group delay behaviour," *International Journal of RF and Microwave Computer-Aided Engineering*, Vol. 30, No. 9, 1–9, Sept. 2020.
34. Ahn, K.-P., R. Ishikawa, and K. Honjo, "Group delay equalized UWB InGaP/GaAs HBT MMIC amplifier using negative group delay circuits," *IEEE Trans. Microw. Theory Techn.*, Vol. 57, No. 9, 2139–2147, Sept. 2009.
35. Ravelo, B., S. Lalléchère, A. Thakur, A. Saini, and P. Thakur, "Theory and circuit modelling of baseband and modulated signal delay compensations with low- and band-pass NGD effects," *Int. J. Electron. Commun. (AEÜ)*, Vol. 70, No. 9, 1122–1127, Sept. 2016.
36. Groenewold, G., "Noise and group delay in active filters," *IEEE Trans. CAS I: Regular Papers*, Vol. 54, No. 7, 1471–1480, Jul. 2007.
37. Hwang, M.-E., S.-O. Jung, and K. Roy, "Slope interconnect effort: Gate-interconnect interdependent delay modeling for early CMOS circuit simulation," *IEEE Trans. CAS I*, Vol. 56, No. 7, 1428–1441, Jul. 2009.